Spike-Timing Dependent Plasticity as a Mechanism for Ocular Dominance Shift

Beth Ann Siegler*
Center for Neuroscience, University of Pittsburgh, Pittsburgh, PA 15260

Maureen Ritchey†
University of Notre Dame, South Bend, IN 46556

Jonathan Rubin‡
Department of Mathematics, University of Pittsburgh, Pittsburgh, PA 15260

January 26, 2004

Abstract. Spike-timing dependent plasticity (STDP) has been implicated in visual cortex modification. We created a model of ocular dominance (OD) shift based on STDP rules and compared it to experimental results. Although STDP proved to be a powerful mechanism for OD shift in our model, we found that it was unable to account for more subtle effects of monocular deprivation.

(Note that all authors contributed equally to this paper.)

Keywords. Spike-timing dependent plasticity, ocular dominance, monocular deprivation, monocular inactivation

1 Introduction

In the mammalian visual system, retinal cells project to two main layers of the cat lateral geniculate nucleus (LGN) - a contralateral layer (Lamina A), which receives input from the opposite side of the brain, and an ipsilateral layer (Lamina A1), which receives input from the eye on the same side of the brain. Geniculate neurons project mainly to Layer IV of the primary visual cortex (V1) in alternating eye-specific columns called ocular dominance (OD) columns. Such a structure consists of a group of cortical cells which preferentially respond to one eye. These columns continue into other layers of cortex. Layer IV afferents project primarily to Layer II/III, in which neurons form connections within the layer and to other cortical layers; see Figure 1a.

A change in the responsiveness of cortical cells to each eye, or OD shift, can be induced by depriving one eye of light (monocular deprivation, or MD). MD causes the OD columns

*bas95@pitt.edu
†mritchey@nd.edu
‡Partially supported by NSF grant DMS-0108857; member of the Center for the Neural Basis of Cognition; rubin@math.pitt.edu

corresponding to the non-deprived eye to expand, while deprived-eye OD columns shrink. These changes have been shown to result from competitive interaction between neurons representing each eye [11]. Postsynaptic activity is necessary for OD shift [15], consistent with Hebbian learning, but the mechanisms through which OD shift occurs remain unclear.

Rittenhouse et al. [16] compared two types of monocular deprivation: monocular inactivation (MI) and monocular suture (MS). In MI, a drug injection prevents the deprived eye's retina from generating action potentials. In MS, the retina generates some spontaneous action potentials, and diffuse light entering through the eyelid induces a low level of futher retinal activation that is uncorrelated with activity in the non-deprived retina. Rittenhouse et al. found that MS creates more of an OD shift in Layer II/III than that which is induced by MI. Since MI more drastically diminishes retinal firing than MS, this result may seem counterintuitive; however, it is consistent with the hypothesis that presynaptic activity is required for OD shift. Computational work has demonstrated previously that spike-timing dependent plasticity (STDP) can lead to the re-establishment of cortical maps after lesions [20]. The goal of this paper is to explore whether both the synaptic weakening and strengthening components of OD shift, and in particular the increased shift in MS relative to MI, could arise through STDP of corticocortical synapses.

In STDP, when a presynaptic cell fires before a postsynaptic cell within a window of tens of milliseconds, the corresponding synapse potentiates, while the opposite ordering leads to synaptic depression (reviewed e.g. in [2]). We implemented a phenomenological STDP rule, modified from [13], in a simplified, eight-cell visual cortical network model consisting of 6 Layer IV cells and 2 Layer II/III cells, grouped into two OD "columns". Under simulated normal conditions, the STDP in the system did not destabilize the imposed OD pattern. STDP proved to be a highly effective mechanism for inducing an OD shift in both MD conditions. It could not, however, account for the experimental disparity between MS and MI results. We conclude that the corticocortical plasticity observed in MD experiments is unlikely to derive from STDP alone.

2 Model and Results

We created a neural network consisting of two cortical layers. Our focus on a cortical network was motivated by the fact that Rittenhouse et al. studied animals at a developmental stage in which geniculocortical synapses (to Layer IV neurons) are no longer plastic, while corticocortical synapses remain modifiable [14]. In our model, each of six Layer IV cells and two recurrently connected Layer II/III cells was assigned to an eye, representing two ocular dominance columns; see Figure 1b. Within a given column, Layer IV cells were of three types in terms of initial synaptic connectivity: one cell connected to both Layer II/III cells (numbered 1, 2 in Figure 1b) but with a much stronger connection to the II/III cell in its column (these are cells 3, 6 in Figure 1b); one cell connected equally strongly to both Layer II/III cells (cells 4, 7 in Figure 1b); and one cell connected only to the II/III cell in its column (cells 5, 8 in Figure 1b). This structure is based on experimental findings that a minority of Layer IV cells project only to II/III cells

within the same OD column [1] and that the degree of ocular dominance is less in Layer II/III than in Layer IV in normal conditions [12].

All synaptic connections in the model were excitatory and were allowed to evolve via STDP. Changes in synaptic strengths within the model were scaled by multiplicative factors (see [22, 17, 18]). In particular, we simulated two forms of limiting factors on synaptic potentiation. In the *heterosynaptic model*, all synapses on one post-synaptic cell compete for a limited pool of trophic factor. Thus, increases in the strength of one synapse onto a cell can limit the possible strengthening of other synapses onto the cell [6]. In the *homosynaptic model*, each synapse has a bound on its strength but bounds on different synapses are independent [3].

The equations in our model are modified from the phenomenological STDP model of Karbowski and Ermentrout [13]. Each neuron is a phase oscillator, represented by $\theta \in [0, 2\pi)$, with its firing frequency modulated significantly by Gaussian noise. When any neuron fires, it induces pulses in an auxiliary variable, s, which serves as a marker for firing time and also drives a slower timing variable u. The combined dynamics of s and u in pre- and postsynaptic cells govern the STDP rule in the model, as shown in Figure 2.

The precise equations in the model take the following forms. For a Layer IV cell,

$$\theta' = \omega + \sigma x, \quad \theta \in [0, 2\pi) \tag{1}$$

with default values $\omega = 0.13$, $\sigma = 0.1$, and with x a Wiener process. The value of ω was altered during the course of simulations to emulate responses to visual stimuli. Under *normal* conditions, stimuli were modeled as Markov processes with fixed on and off probabilities. During the duration of a stimulus, ω was switched to 1, leading to rapid spiking. For simplicity, in the normal case, all patterns were assumed to affect all Layer IV cells identically, leading to the same increase in firing rate during the same time period. An example is illustrated in Figure 3 (top). In *monocular inactivation* (MI), Layer IV cells correponding to the inactivated eye did not respond to patterns; moreover, to simulate the elimination of retinal spontaneous activity, we decreased ω to 0.09 in these cells. See Figure 3 (middle). In *monocular suture* (MS), the deprivation of one eye cannot be assumed to be absolute. Thus, Layer IV cells corresponding to the sutured eye fired in response to patterns, but with fewer spikes and only after a delay [23]. For simplicity, in the simulations shown, these cells responded to patterns with a single spike at the end of the pattern; see Figure 3 (bottom).

For a Layer II/III cell,

$$\theta_i' = \omega_i + \rho \sum_j g_{ji} s_j \tag{2}$$

with $\omega_i = 0.01$, to simulate weaker firing in Layer II/III than in Layer IV [4, 7], with $\rho = 0.3$, and with the sum over cells presynaptic to cell i, with synaptic strengths g_{ji}. The term s_j ensures that the synaptic inputs from a given presynaptic cell are only active for a short time after the cell spikes (see below). Synaptic strengths evolve via

$$g_{ji} = \alpha(s_i u_j - \delta s_j u_i) g_{ji} F_{compete}, \; i \in \{1, 2\} \tag{3}$$

where $\alpha = 0.0001$ and $\delta = 1.5$. Note that i only takes the values 1 or 2 because only the Layer II/III cells receive synaptic input in the model. The product $s_i u_j$ in equation (3) induces potentiation when a presynaptic cell spikes before its postsynaptic target, while the term $s_j u_i$ gives depression upon post- before presynaptic firing; see Figure 2. The term $F_{compete}$ in equation (3) takes a different form depending on whether we implement the heterosynaptic or homosynaptic model. In the heterosynaptic case, $F_{compete} = M_i - \sum_j g_{ji}$ to encode competition among all synapses on the same postsynaptic cell; we took $M_i = 2$ independent of i. In the homosynaptic case, $F_{compete} = M_{ji} - g_{ji}$; we took all $M_{ji} = 1.25$.

Finally, we set $s_j = \sqrt{\beta}\exp(-\beta(1-\cos(\theta_j)))$ with $\beta = 75$, such that cell j induces synaptic responses of short duration when θ_j reaches 2π (from below, before being reset to 0), and took

$$u_j' = -u_j/\mu + s_j \tag{4}$$

as a filtered version of s_j. In equation (4), $\mu = 3$ except during stimuli, when $\mu = 30$ to smooth out the time course of u_j. The particular parameters selected yield an STDP window of about 20 msec for LTP and LTD from single spike pairs. Figure 4 shows a numerical example of how s, u interact.

As seen in Figure 3, our model (1)-(4) produces different firing patterns in normal, MI, and MS conditions. The experimental manipulations in MI and MS were taken to occur in the eye corresponding to the OD column including cells 1, 3, 4, and 5 (Figure 1b). Initially, g_{31}, g_{51} are strong, corresponding to connections from the Layer IV cells projecting preferentially to cell 1. In the course of each simulation, all weights g_{ji} are free to evolve. Figure 5 illustrates the evolution of synaptic weights g_{31} and g_{61} in each scenario, where g_{61} corresponds to an input to the deprived OD column from the unaltered OD column in the MI and MS cases. Note that the weights are stable in the normal case but that STDP induces a strong shift in the MI and MS cases. While the heterosynaptic model was used here, similar results occurred in the homosynaptic model, except that connections from the non-deprived OD column to the Layer II/III cell on the deprived side, such as g_{61}, did not strengthen much above their normal levels in the MI/MS cases. Nonetheless, weights such as g_{61} did rise well above weights within the deprived OD column, such as g_{31}, in these cases, and thus these results would have been classified as a strong OD shift in an experimental study.

Results from 20 simulations of each case, for both models, are summarized in Table 1 as mean $\pm$ standard deviation; values below 10^{-4} are denoted by **. These simulations were each run for 200000 time units using XPPAUT [8]. Although in some simulations there appeared to be futher evolution of weights beyond time 200000, the qualitative results and relative levels of the weights appeared to remain consistent beyond this time. Values for g_{31}, g_{61} are shown in bold font to emphasize the OD shift. If OD shift is measured by comparing the ratio g_{61}/g_{31} in the normal case to that in the MI or MS case, then the results show an increased OD shift in MS than in MI, as in [16]. The OD shift seen in Table 1 in the MI case exceeds that found experimentally, however.

Table 1: Asymptotic Weights						
weight	normal (hetero)	MI (hetero)	MS (hetero)	normal (homo)	MI (homo)	MS (homo)
g_{21}	$.0016 \pm .0014$	**	**	$.00030 \pm .00024$	$.00040 \pm .00033$	$.00034 \pm .00033$
g_{31}	$\mathbf{.5764 \pm .2106}$	$\mathbf{.00021 \pm .00032}$	**	$\mathbf{.5573 \pm .2440}$	$\mathbf{.0017 \pm .0016}$	$\mathbf{.00051 \pm .00033}$
g_{41}	$.1180 \pm .0759$	**	**	$.1217 \pm .0942$	$.00016 \pm .00012$	**
g_{51}	$.5250 \pm .2389$	$.00021 \pm .00022$	**	$.5979 \pm .2737$	$.0013 \pm .0010$	$.00092 \pm .00069$
g_{61}	$\mathbf{.0903 \pm .0597}$	$\mathbf{.2740 \pm .3356}$	$\mathbf{.2502 \pm .2629}$	$\mathbf{.1173 \pm .0597}$	$\mathbf{.1332 \pm .1197}$	$\mathbf{.1248 \pm .0617}$
g_{71}	$.1194 \pm .0775$	$.2043 \pm .2459$	$.1939 \pm .2009$	$.1236 \pm .0757$	$.1167 \pm .0775$	$.1615 \pm .1232$
g_{12}	$.0019 \pm .0016$	$.0014 \pm .0019$	$.00091 \pm .00078$	$.00031 \pm .00034$	$.00022 \pm .00020$	$.00028 \pm .00029$
g_{32}	$.1189 \pm .0729$	$.00095 \pm .00101$	$.00057 \pm .00058$	$.1637 \pm .1035$	$.00015 \pm .00011$	$.00010 \pm .00005$
g_{42}	$.0963 \pm .0377$	$.0010 \pm .0011$	$.00057 \pm .00073$	$.1412 \pm .0984$	$.00016 \pm .00011$	**
g_{62}	$.6006 \pm .2630$	$.5747 \pm .3205$	$.6085 \pm .3212$	$.6435 \pm .2149$	$.4753 \pm .2297$	$.8700 \pm .3517$
g_{72}	$.0902 \pm .0485$	$.0876 \pm .0555$	$.1148 \pm .0525$	$.1465 \pm .0911$	$.1294 \pm .1004$	$.1224 \pm .0807$
g_{82}	$.5171 \pm .2109$	$.6786 \pm .3365$	$.6645 \pm .3602$	$.6070 \pm .2061$	$.5772 \pm .1533$	$.5297 \pm .1992$

As a numerical check, note that in the normal case, the two columns (cells 1,3,4,5 and cells 2,6,7,8; see Figure 1b) should behave similarly, and weights of connections that occupy analogous positions on each side of the network should attain similar levels. This is borne out in the data of Table 1 (compare (g_{51}, g_{82}); (g_{31}, g_{62}); (g_{61}, g_{32}); (g_{41}, g_{72}); (g_{71}, g_{42}); (g_{21}, g_{12}) in the normal cases).

A key point to note in Figure 5 is that the weakening of g_{31}, the IV-II/III connection within an OD column, always precedes the strengthening of g_{61}, when an OD shift occurs. The weakening occurs initially because there is a bias toward LTD in the STDP model (e.g. [21]). Under normal conditions, bursts of spikes fired by cell 3 in Layer IV in response to stimuli can drive the firing of the Layer II/III cell 1, which compensates for this bias. Once these responses are removed, the firing of cell 3 is mostly uncorrelated from that of cell 1, and the bias toward LTD can take over. This bias is independent of the form of synaptic bounding mechanism, heterosynaptic or homosynaptic, and indeed we find that how this is modelled does not significantly impact the MI/MS results. Since the Layer IV cell 6 from the nondeprived column still bursts in MI/MS, it gains an advantage at driving cell 1, although this is initially small, because g_{61} is so small. Eventually, this advantage translates into further weakening of g_{31} and strengthening of g_{61}. This rise in g_{61} is consistent with modeling work on the formation of cortical maps [20].

3 Discussion

Spike-timing dependent plasticity has been implicated in visual cortex plasticity [19, 9]; however, it has not been modeled previously in the context of ocular dominance shift. We found that STDP produces massive OD shifts, as typify monocular deprivation experiments. STDP alone does not appear to account for differences in OD shift between MI and MS deprivation paradigms, however [16]. This inability to distinguish between MI and MS indicates that other mechanisms, either in conjunction with STDP or on their own, may take part in driving OD shift and particularly in limiting it in MI conditions.

Because STDP without multiplicative scaling can lead to unbounded synaptic strengthening [22, 17, 18], we experimented with two ways of reining in runaway synapses. With a heterosy-

naptic mechanism, several presynaptic cells synapsing on a single postsynaptic cell compete for a limited amount of necessary trophic factor [10]. Alternatively, with a homosynaptic mechanism, bounds are placed on each individual synapse, which potentiates or depresses according to the level of temporal correlation of pre- and postsynaptic spiking. Note that Rittenhouse et al. [16] came to the conclusion that a homosynaptic rule plays a role in OD shift. In our simulations, STDP yielded qualitatively similar results with either bounding scheme, even under variations in the values of the bounds used (data not shown).

It is theoretically possible that a different form of STDP model would yield different computational results from what we have observed. Note that Froemke and Dan found that when multiple pre- and postsynaptic spikes occur within a window of tens of milliseconds, the first spike interaction dominates the resulting STDP outcome [9], while Sjöström et al. found that LTP dominates in these situations [19]. These disparities only relate to STDP when multiple spikes occur during a short time window, however. In our simulations, such rapid spiking only occurs when Layer IV cells respond to visual stimuli. The accelerated spiking does not generally produce multiple Layer II/III spikes in our simulations, so alternative means of handling multi-spike interactions should not significantly impact our results. Also, our results are consistent with previous work on STDP and directional selectivity in the visual cortex, which suggests that STDP of synaptic strength alone is insufficient to allow for the emergence and maintainance of experimentally observed properties [5]. Finally, note that we chose certain ω values to speed convergence of our simulations (via a high level of spontaneous activity in Layer IV and a low level of spontaneous activity in Layer II/III, which emphasized the effects of STDP). While the accelerated convergence did not appear to affect qualitative outcomes, further study is warranted to explore the effects of parameter choices more thoroughly.

Figure Captions

Figure 1: a) Diagram of the feline visual system. b) Schematic illustration of the cells in our network model, with lines representing excitatory synaptic connections and line thicknesses corresponding to initial synaptic strengths in simulations.

Figure 2: Cartoon of the phenomenological STDP rule [13]. Solid curves correspond to time course of s, dashed curves to u, for each cell. Left: When a presynaptic cell (j) fires before a postsynaptic one (i), s_i, u_j line up to give LTP (dotted line). Right: When a presynaptic cell fires after a postsynaptic one, s_j, u_i line up to give LTD (dotted line).

Figure 3: Example firing patterns in normal (top), MI (middle), and MS (bottom) scenarios. θ is plotted on $[0, 2\pi)$, so that when θ reaches 2π, a spike occurs and θ is effectively reset to 0 (with no jump in θ').

Figure 4: Example of the behavior of model variables during a simulation. a) The solid curve corresponds to u for a presynaptic cell (call it u_{pre}), while the two vertical dashed segments correspond to s for a postsynaptic cell (call it s_{post}). b) The solid curve is θ_{pre}, while the dashed is θ_{post}. Spikes occur at $\theta = 2\pi$. Note that around time 120, a presynaptic spike occurs just before a postsynaptic one (see b), leading to a temporal overlap of u_{pre} with s_{post} (see a). This yields LTP, but none of the other spikes shown do. Note also that the presynaptic cell experiences a visual stimulus around time 150, yielding three spikes in rapid succession (see b).

Figure 5: Evolution of synaptic weights. The heterosynaptic synaptic bounding model was used here. Note the different timescales in different plots. a) Normal conditions. The solid curve corresponds to g_{31}, the weight of a synapse within an OD column, while the dashed curve corresponds to g_{61}, the weight of a synapse across OD columns. b) MI conditions. c) MS conditions. In b),c), g_{31} connects cells within the deprived column.

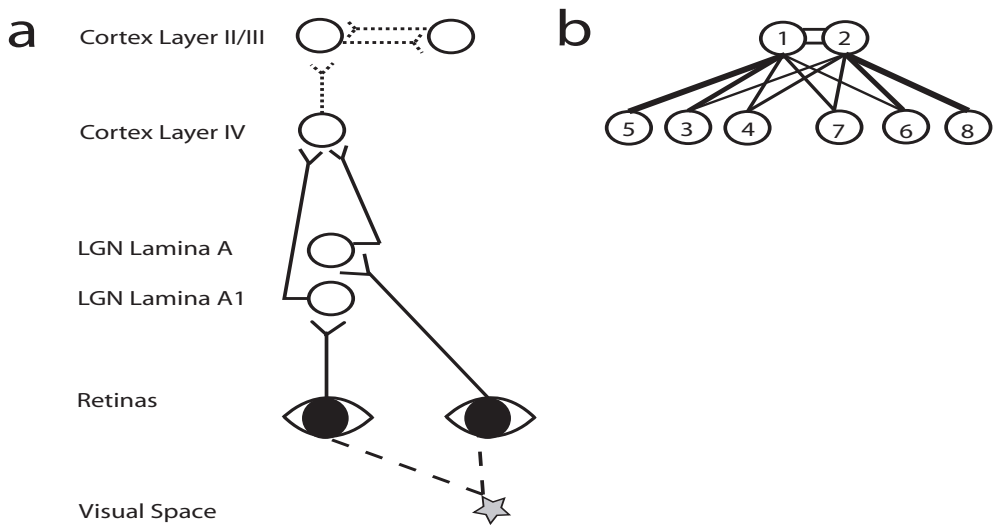
a
Cortex Layer II/III
Cortex Layer IV
LGN Lamina A
LGN Lamina A1
Retinas
Visual Space
b
1
2
5
3
4
7
6
8

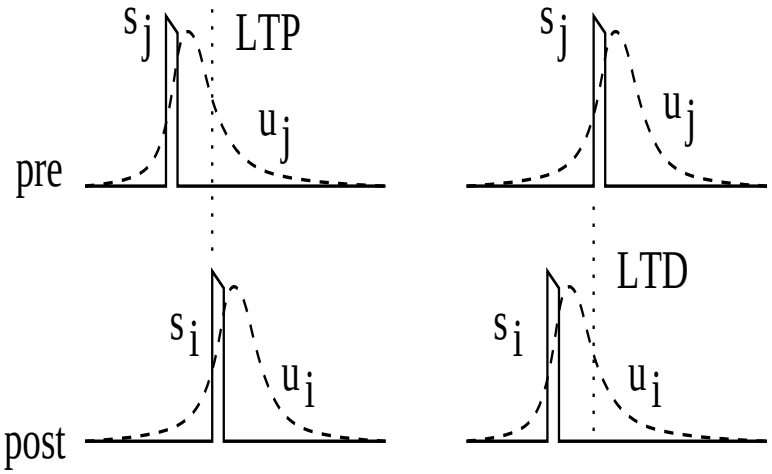

Figure 2

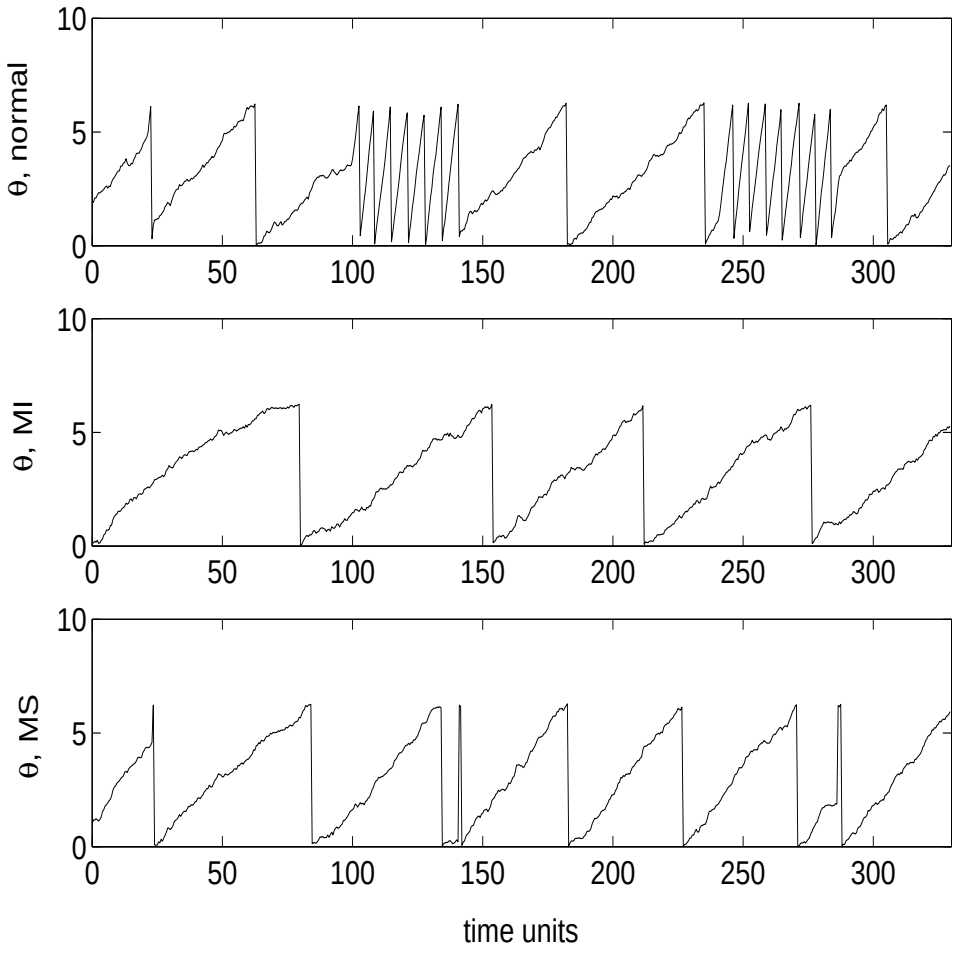

Figure 3

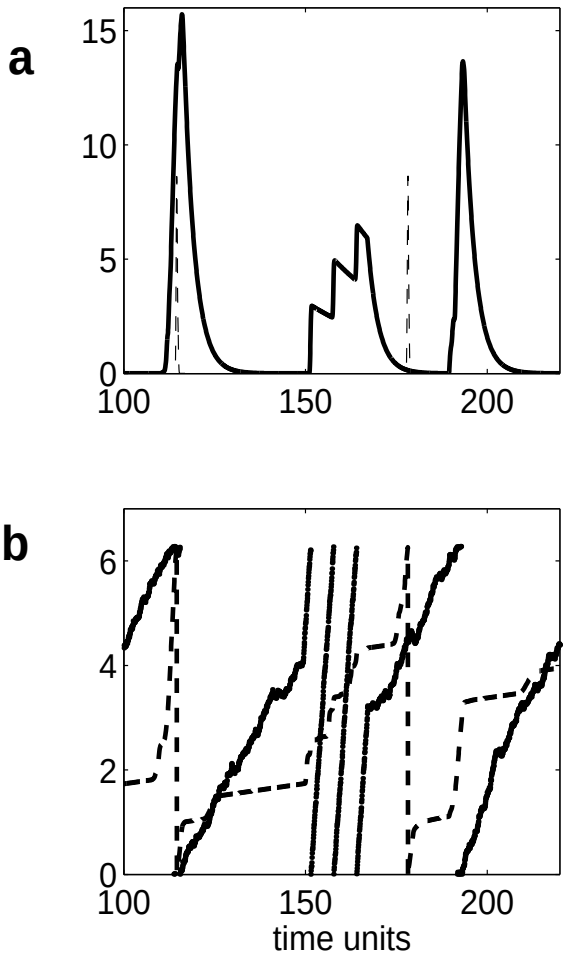

Figure 4

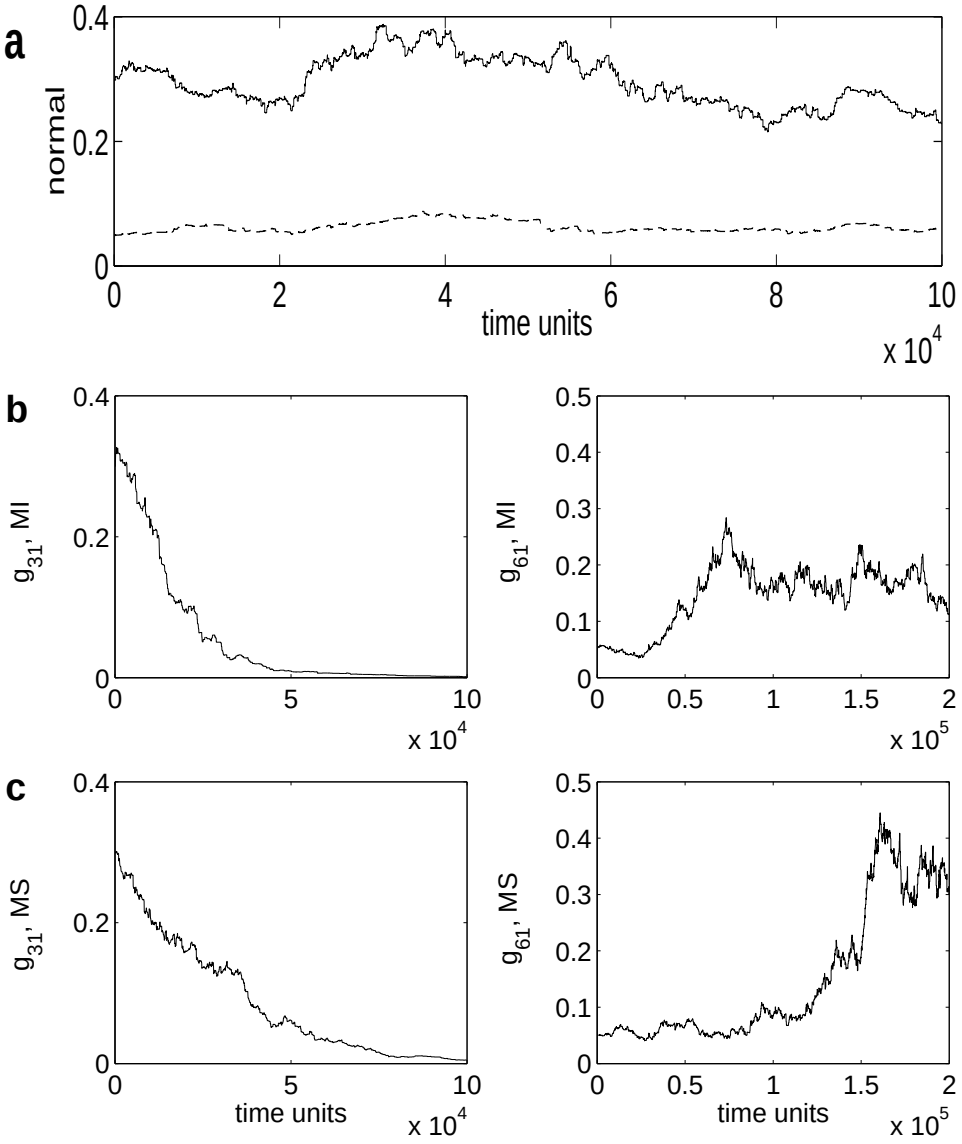
a
normal
0.4
0.2
0
0
2
4
6
8
10
time units
x 10^4
b
g31, MI
0.4
0.2
0
0
5
10
x 10^4
g61, MI
0.5
0.4
0.3
0.2
0.1
0
0
0.5
1
1.5
2
x 10^5
c
g31, MS
0.4
0.2
0
0
5
10
time units
x 10^4
g61, MS
0.5
0.4
0.3
0.2
0.1
0
0
0.5
1
1.5
2
time units
x 10^5

Figure 5

References

[1] N. Berman, B. Payne, D. Labar, and E. Murphy. Functional organization of neurons in cat striate cortex: variations in ocular dominance and receptive-field type with cortical laminae and location in visual field. *J. Neurophysiol.*, **48**:1362–1377, 1982.

[2] G. Bi. Spatiotemporal specificity of synaptic plasticity: cellular rules and mechanisms. *Biol. Cybern.*, **87**:319–332, 2002.

[3] E. Bienenstock, L. Cooper, and P. Munro. Theory for the development of neuron selectivity: orientation specificity and binocular interaction in visual cortex. *J. Neurosci.*, **2**:32–48, 1982.

[4] J. Brumberg, D. Pinto, and D. Simons. Cortical columnar processing in the rat whisker-to-barrel system. *J. Neurophysiol.*, **82**:1808–1817, 1999.

[5] N. Buchs and W. Senn. Spike-based synaptic plasticity and the emergence of direction selective simple cells: simulation results. *J. Comput. Neurosci.*, **13**:167–186, 2002.

[6] G. Carmignoto, R. Canella, P. Candeo, M. Cormelli, and L. Maffei. Effects of nerve growth factor on neuronal plasticity of the kitten visual cortex. *J. Physiol.*, **464**:343–360, 1993.

[7] D.Feldmeyer, J. Lubke, A. Silver, and B. Sakmann. Synaptic connections between layer 4 spiny neurone-layer 2/3 pyramidal cell pairs in juvenile rat barrel cortex: physiology and anatomy of interlaminar signalling within cortical columns. *J. Physiol.*, **538**:803–822, 2002.

[8] B. Ermentrout. *Simulating, Analyzing, and Animating Dynamical Systems*. SIAM, Philadelphia, 2002.

[9] R. Froemke and Y. Dan. Spike-timing-dependent synaptic modification induced by natural spike trains. *Nature*, **416**:433–438, 2002.

[10] D. Gillespie, M. Crair, and M. Stryker. Neurotrophin-4/5 alters responses and blocks the effect of monocular deprivation in cat visual cortex during the critical period. *J. Neurosci*, **20**:9174–86, 2000.

[11] R. Guillery and D. Stelzner. The differential effects of unilateral lid closure upon the monocular and binocular segments of the dorsal lateral geniculate nucleus in the cat. *J. Comp. Neurol.*, **148**:417–422, 1970.

[12] D. Hubel and T. Wiesel. Receptive fields of cells in striate cortex of very young, visually inexperienced kittens. *J. Neurophysiol.*, **26**:994–1002, 1963.

[13] J. Karbowski and G. Ermentrout. Synchrony arising from a balanced synaptic plasticity in a network of heterogeneous neural oscillators. *Phys. Rev. E*, **65**:0319021–0319025, 2002.

[14] S. Levay, T. Wiesel, and D. Hubel. The development of ocular dominance columns in normal and visually deprived monkeys. *J. Comp. Neurol.*, **191**, 1980.

[15] H. Reiter and M. Stryker. Neural plasticity without postsynaptic action potentials: less-active inputs become dominant when kitten visual cortical cells are pharmacologically inhibited. *Proc. Natl. Acad. Sci. U S A*, **85**:3623–3627, 1988.

[16] C. Rittenhouse, H. Shouval, M. Paradiso, and M. Bear. Monocular deprivation induces homosynaptic long-term depression in visual cortex. *Nature*, **397**:347–350, 1999.

[17] J. Rubin. Steady states in an iterative model for multiplicative spike-timing dependent plasticity. *Network: Comput. Neural Sys.*, **12**:131–140, 2001.

[18] J. Rubin, D. Lee, and H. Sompolinsky. Equilibrium properties of temporally asymmetric Hebbian plasticity. *Phys. Rev. Lett.*, **86**:364–367, 2001.

[19] P. Sjostrom, G. Turrigiano, and S. Nelson. Rate, timing, and cooperativity jointly determine cortical synaptic plasticity. *Neuron*, **32**:1149–1164, 2001.

[20] S. Song and L. Abbott. Cortical development and remapping through spike timing-dependent plasticity. *Neuron*, **13**:339–350, 2001.

[21] S. Song, K. Miller, and L. Abbott. Competitive hebbian learning through spike-timing-dependent synaptic plasticity. *Nat. Neurosci.*, **3**:919–926, 2000.

[22] M. van Rossum, G. Bi, and G. Turrigiano. Stable hebbian learning from spike timing-dependent plasticity. *J. Neurosci.*, **20**:8812–8821, 2000.

[23] X. Zhan, C. Cox, J. Rinzel, and S. Sherman. Current clamp and modeling studies of low-threshold calcium spikes in cells of the cat's lateral geniculate nucleus. *J. Neurophysiol.*, **81**:2360–2373, 1999.